Electrochemical CO2 Reduction with a Heterogenized Iridium-Pincer Catalyst in Water

Jonathan De Tovar, Ashta C. Ghosh, Tom Di Santo, Mathieu Curtil, Dmitry Aldakov, Matthieu Koepf, Marcello Gennari

ChemCatChem

Research Article
doi.org/10.1002/cctc.202300049

Chemistry Europe
European Chemical Societies Publishing

www.chemcatchem.org

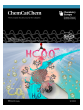

Electrochemical CO_2 Reduction with a Heterogenized Iridium–Pincer Catalyst in Water

Jonathan De Tovar,[a, b] Ashta C. Ghosh,[a, b] Tom Di Santo,[b] Mathieu Curtil,[b] Dmitry Aldakov,[c] Matthieu Koepf,*[a] and Marcello Gennari*[b]

Immobilization of well-defined homogenous (electro)catalysts onto conductive supports offers an attractive strategy for designing advanced functional materials for energy conversion. In this context, this study reports (i) the introduction of a pyrene anchoring group on a PNP–pincer Ir^{I} complex previously described as a selective catalyst for the electrodriven CO_2 reduction (CO_2RR) into CO in DMF/water mixtures, (ii) the comparison of its CO_2RR activity in DMF/water mixtures with the ones of two pyrene-free reference complexes, and (iii) its activity in pure water after immobilization onto carbon nanotubes (CNTs). Surprisingly, in homogeneous conditions we find $HCOO^-$, instead of CO, as the main CO_2 reduction product for the three catalysts. After immobilization on CNTs, even if non-negligible competitive proton reduction reaction is observed in fully aqueous media, the complex is still able to drive CO_2RR and produce $HCOO^-$ with a significantly lower overpotential with respect to solution studies.

Introduction

Direct electrochemical conversion of carbon dioxide into fuels and chemicals offers attractive prospects for the transition towards a sustainable "low-carbon" economy, and thus, is currently a domain of intense research.[1] In this field, the immobilization of well-defined transition metal complexes able to drive the CO_2 Reduction Reaction (CO_2RR) onto conductive supports is an appealing strategy.[2] Indeed, heterogenized molecular catalysts often combine the benefits of heterogeneous catalysis[3] (catalyst recyclability, efficient electron transfer from the electrode support to the catalytic centers) with those of homogenous catalysis[4] (uniform catalytic sites, high control on the active site properties and tunability, simpler mechanistic investigations and relative ease to establish structure-activity correlations). Furthermore, it can drastically reduce drawbacks typical of homogeneous catalysts, like their diffusion-dependent kinetics and poor stability. The immobilization of a molecular catalyst can indeed help preventing its fast deactivation under turnover conditions by limiting its free diffusion in the bulk and the occurrence of detrimental intermolecular reactions involving highly reactive intermediates (dimerization, ligand degradation) or its poisoning with reaction products.[2b,5] Besides, once heterogenized, the catalyst of interest can be used regardless of its intrinsic solubility into the media selected, sometimes allowing to promote a remarkable new reactivity.[6] Heterogenization can, thus, offer an interesting approach for transposing commonly used catalysts from organic to aqueous conditions that are generally more desirable for the development of functional devices, while potentially broadening their scope of activity.

When the heterogenization of a molecular CO_2RR catalyst is targeted, the nature of the catalyst and that of the supporting material, as well as the immobilization strategy have to be attentively planned.

The choice of multi-walled carbon nanotubes (MWCNTs) as supporting material is attractive since it combines an excellent electrical conductivity and porosity of the substrate with the possibility to easily functionalize it through non-covalent π-π stacking interactions. This anchoring mode does not affect the conductivity of MWCNTs and can result in excellent loading densities and surface stability of the complexes.[7] Significant precedents of CO_2RR catalysts immobilized on carbon nanotubes by π-π stacking interactions include manganese–bipyridine,[2b] nickel–cyclam,[8] iron-, copper-, cobalt- and nickel-complexes of porphyrins[2c,d] and phthalocyanines,[2c,d,9] and rhenium–diimine[10] complexes. In all these systems, working in aqueous or mixed organic/water medium, heterogenization allowed for a significant enhancement of the catalytic activity and/or stability of the catalysts compared to the homogeneous counterparts.

Concerning the nature of the molecular catalyst to be immobilized, we focus here on iridium–pincer complexes. Metal–pincer complexes are potentially attractive for electrocatalytic CO_2RR since they incorporate tridentate redox non-innocent ligands that can allow for the stabilization of critical

[a] Dr. J. De Tovar, Dr. A. C. Ghosh, Dr. M. Koepf
Université Grenoble Alpes, CNRS, CEA, IRIG, Laboratoire de Chimie et Biologie des Métaux
Grenoble F-38000 (France)
E-mail: matthieu.koepf@cea.fr
[b] Dr. J. De Tovar, Dr. A. C. Ghosh, T. Di Santo, M. Curtil, Dr. M. Gennari
Département de Chimie Moléculaire, Univ. Grenoble Alpes, UMR CNRS 5250
38000 Grenoble (France)
E-mail: marcello.gennari@univ-grenoble-alpes.fr
[c] Dr. D. Aldakov
Université Grenoble Alpes, CEA, CNRS, INP, IRIG/SyMMES
38000 Grenoble (France)

Supporting information for this article is available on the WWW under https://doi.org/10.1002/cctc.202300049

catalytic intermediates. Iridium complexes are known as CO_2 reduction electrocatalysts since late 90s,[11] but the introduction of pincer ligands to support this activity has only been proposed by Brookhart *et al.* in 2012.[12] In this seminal work an iridium(III) dihydride complex featuring an anionic PCP–pincer ligand was demonstrated to be a selective electrocatalyst for the production of $HCOO^-$ in acetonitrile/water mixtures. A later extension of this work demonstrated the versatility of pincer ligand platforms for designing fully water-soluble catalysts.[13] Finally, one of the Brookhart complexes was successfully integrated onto carbon nanotube-coated gas diffusion electrodes (GDEs) by non-covalent binding, leading to a remarkable increase of turnover number from 40 to $2 \cdot 10^5$ while maintaining the selectivity of the complex for formate production.[14]

Given this promising precedent, we decided to extend this strategy to a PNP pincer-supported Ir^I complex (**Ir^H**, Scheme 1) recently described by Brudvig *et al.* as a selective electrocatalyst for CO_2 reduction to CO in DMF/water mixtures.[15] In the following, we thus report (i) the functionalization of the ligand scaffold with a pyrene anchoring group and its complexation to the Ir^I center; (ii) the comparison of the CO_2RR activity of the pyrene-tagged complex (**Ir^{OPyr}**, Scheme 1) in DMF/water mixtures with the activity of the two reference complexes **Ir^H** and **Ir^{OMe}**, the latter being substituted with a methoxy group in the *para*-position of the pyridine ring of the pincer (Scheme 1); and (iii) the immobilization of **Ir^{OPyr}** on MWCNTs to perform CO_2RR catalysis in fully aqueous medium.

Interestingly, using a mercury (Hg) pool working electrode we observe the formation of $HCOO^-$ as the main reduction product (instead of CO, as previously reported for **Ir^H** using carbon paper working electrode)[15] for the three catalysts tested in homogeneous conditions. Gratifyingly, the selective generation of $HCOO^-$ is retained after immobilization of the pyrene-tagged complex even in pure water, together with a significant decrease of the CO_2RR overpotential.

Results and Discussion

Synthesis

In order to prepare iridium–PNP@MWCNTs hybrids, the first step was the introduction of a pyrene anchoring group on the periphery of the PNP–pincer. More specifically, the **PNP^H** ligand framework shown in Scheme 1 was substituted in the *para*-position of the pyridine ring with a butylpyrene tag to afford

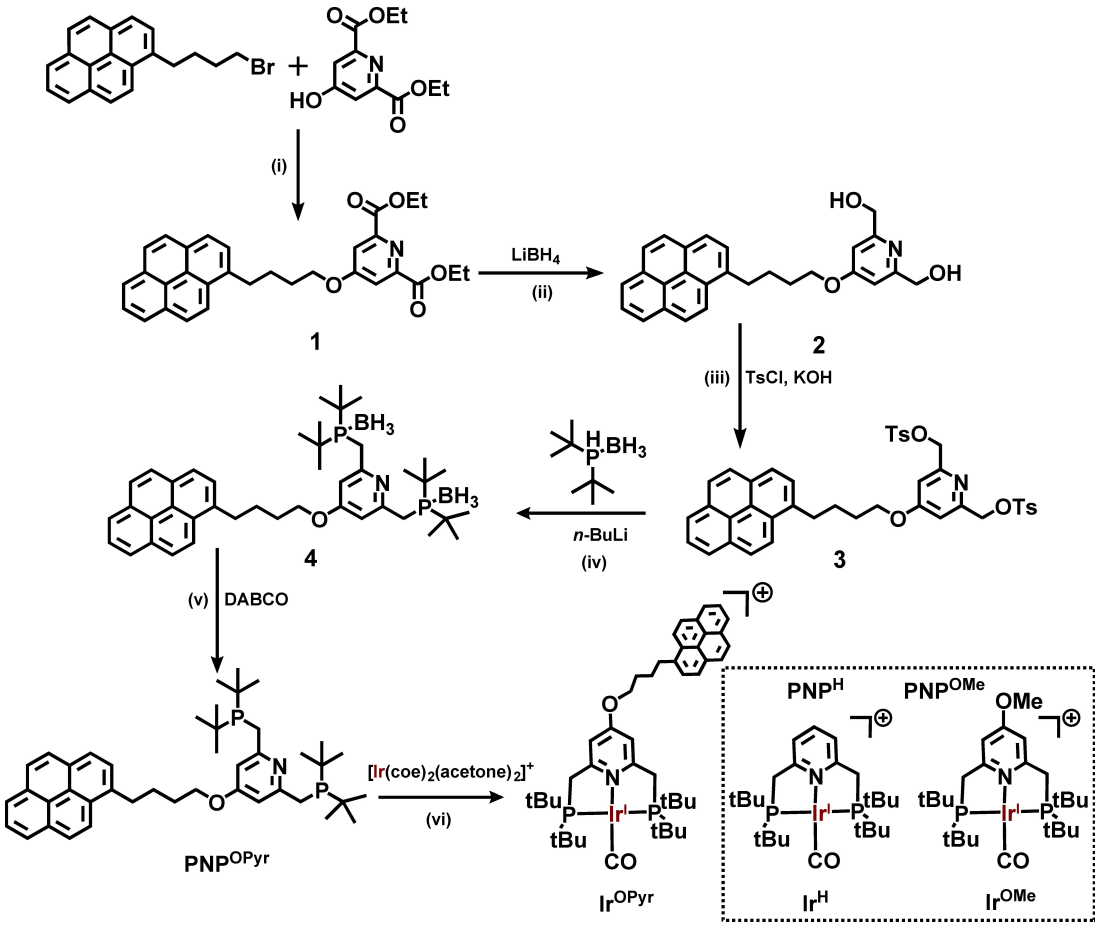

Scheme 1. Multi-step synthesis of the ligand **PNP^{OPyr}** and complexation: (i) K_2CO_3, MeCN, reflux overnight, 64%; (ii) THF:MeOH 5:2, from 0 °C to 60 °C, 1 h, 95%; (iii) KOH, THF, reflux 20 h, 77%; (iv) THF (CH_2Cl_2), from −78 °C to RT overnight, 83%; (v) toluene, 80 °C, 48 h, 60%; (vi) acetone, 30 min, CO bubbling, 68%. The reference complexes **Ir^H**[15] and **Ir^{OMe}** are depicted in the inset.

the **PNP^{OPyr}** ligand via the strategy displayed in Scheme 1 and briefly described thereafter. In the first step, 1-(4-bromobutyl)-pyrene was reacted with diethyl 4-hydroxypyridine-2,6-dicarboxylate to afford derivative **1**, wherein the pyrene and pyridine moieties are linked by an ethereal bond, via a classical Williamson-type reaction. Next, selective reduction of the ethyl ester groups by $LiBH_4$ followed by tosylation of the resulting diol yielded the electrophilic species **3** that can easily undergo nucleophilic substitution by bis-*tert*-butyl phosphine–borane to afford **4**. The final ligand **PNP^{OPyr}** was isolated after deprotection of the phosphines in the presence of 1,4-diazabicyclo[2.2.2]octane (DABCO) as BH_3-scavenger. The overall yield of this five-steps synthesis is of 23% from 1-(4-bromobutyl)-pyrene.

The preparation of the novel Ir^{I}–carbonyl pincer complexes, **Ir^{OPyr}** and **Ir^{OMe}**, was inspired by the synthesis of the unsubstituted **Ir^{H}** complex.[15] The complexes were obtained in good yields (68–70%) by mixing the respective ligands with the Ir^{I} precursor $[Ir(coe)_2(acetone)_2]PF_6$ in acetone before treating the mixture with CO. The formation of the metal–carbonyl adducts was confirmed by the observation of distinctive bands in the infrared spectrum of the compounds, centered at 1952 cm^{-1}, 1956 cm^{-1}, and 1962 cm^{-1}[16] for **Ir^{OPyr}**, **Ir^{OMe}**, and **Ir^{H}**, respectively, and corresponding to the stretching mode of metal-bound CO. The trend observed for the CO frequencies (i.e. a 4–10 cm^{-1} decrease from **Ir^{H}** to **Ir^{OR}**) is in good agreement with an increase of the donor character of the ligands from **PNP^{H}** to **PNP^{OR}** (R = Me or "Pyr"). Similarly to the **Ir^{H}** parent compound, both **Ir^{OR}** complexes display a plane of symmetry orthogonal to the pyridine plane, as attested by the presence of only one singlet in their ^{31}P NMR spectra.

Redox properties of the Ir complexes

The electrochemical properties of the complexes were investigated by Cyclic Voltammetry (CV) in DMF solutions at 0.5 mM with 0.1 M nBu_4NPF_6 supporting electrolyte under Ar atmosphere, using glassy carbon (GC) as the working electrode (Figure 1 and Table 1). In the following, all potentials are referred to the $Fc^{+/0}$ couple. First, we focused on the **Ir^{H}** and **Ir^{OMe}** reference complexes lacking the pyrene moiety (Figure 1). In good agreement with the previous report,[15] the CV of the unsubstituted **Ir^{H}** exhibits an irreversible reduction peak centered at $Ep_c = -2.09$ V that can be attributed to the first monoelectronic reduction of the {(PNP)Ir} unit. Unsurprisingly, the first reduction occurs at a more cathodic potential for the **Ir^{OMe}** complex, with $Ep_c = -2.38$ V, due to the stronger donor character of the methoxy-substituted ligand. Next, we investigated the pyrene-tagged **Ir^{OPyr}** complex. In the cathodic direction, the CV displays two fully irreversible processes at $Ep_{c1} = -2.25$ V and $Ep_{c2} = -2.40$ V followed by a reversible system at $E_{1/2} = -2.52$ V ($\Delta Ep = 92$ mV). The linear dependence of the latter peak's intensity to the square root of the scan rate (Figure S1), confirms that the process is diffusion-controlled and excludes the observation of adsorbed species under the present conditions. A comparison with the CV of pure pyrene under the same conditions ($E_{1/2} = -2.50$ V, $\Delta Ep = 98$ mV, see Supporting Information, Figure S2), permits to assign the reversible cathodic peak of **Ir^{OPyr}** to the one-electron reduction of the pyrene moiety. The first two irreversible cathodic peaks ($Ep_{c1} = -2.25$ V, $Ep_{c2} = -2.40$ V) are thus attributed to the one-electron reduction of the {(PNP)Ir} unit (see DFT calculations below). The splitting of the electrochemical signature of **Ir^{OPyr}** in two cathodic peaks is not observed in the case of **Ir^{H}** and **Ir^{OMe}**, therefore it must be related to the presence of the pyrene tag. More specifically, we tentatively attribute this splitting to the existence an equilibrium in the system related either to the presence of two conformations of the **Ir^{OPyr}**[17] or labile aggregates in the electrolyte.

DFT calculations performed on the three complexes support the assignments of the cathodic peaks observed in the CVs. The structures of **Ir^{OPyr}**, **Ir^{OMe}**, and **Ir^{H}**, were optimized using ORCA starting from Avogadro 3D-built structures and the frontiers orbitals were then calculated (Figure 2 and Table 2). We found that **Ir^{OMe}** and **Ir^{H}** have quite similar LUMOs with an electronic distribution largely delocalized over both the Ir center and the

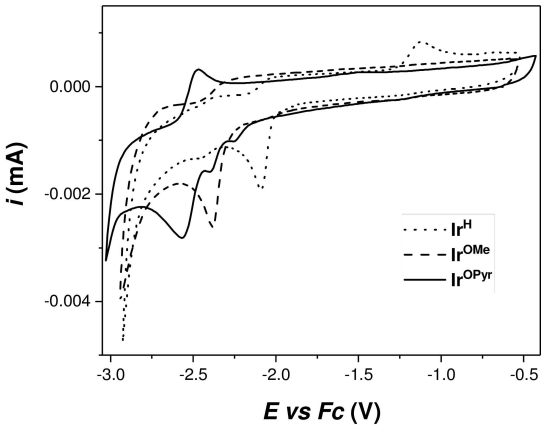

Figure 1. CVs of the three Ir complexes investigated (0.5 mM) in DMF 0.1 M nBu_4NPF_6 under argon (1.6 mm diameter GC working electrode, 100 $mV \cdot s^{-1}$ scan rate).

Table 1. Reduction potentials recorded for the three Ir complexes and pyrene reference under argon in DMF 1 M nBu_4NPF_6.

Species	Reduction(s) [V]
Ir^{H}	−2.09 [a]
Ir^{OMe}	−2.38 [a]
Ir^{OPyr}	−2.25,[a] −2.40,[a] −2.52 (92) [b]
pyrene	−2.50 (98)[b]

Potentials reported vs $Fc^{+/0}$. [a] $Ep_{c,}$ [b] $E_{1/2}$ (ΔE_p).

Table 2. Calculated HOMO, LUMO and LUMO+1 energy for the three Ir complexes.

Complex	HOMO [eV]	LUMO [eV]	LUMO+1 [eV]	$\Delta_{HOMO-LUMO}$ [eV]
Ir^{H}	−5.838	−2.069	−1.184	3.769
Ir^{OMe}	−5.796	−1.757	−1.148	4.039
Ir^{OPyr}	−5.597	−1.858	−1.752	3.739

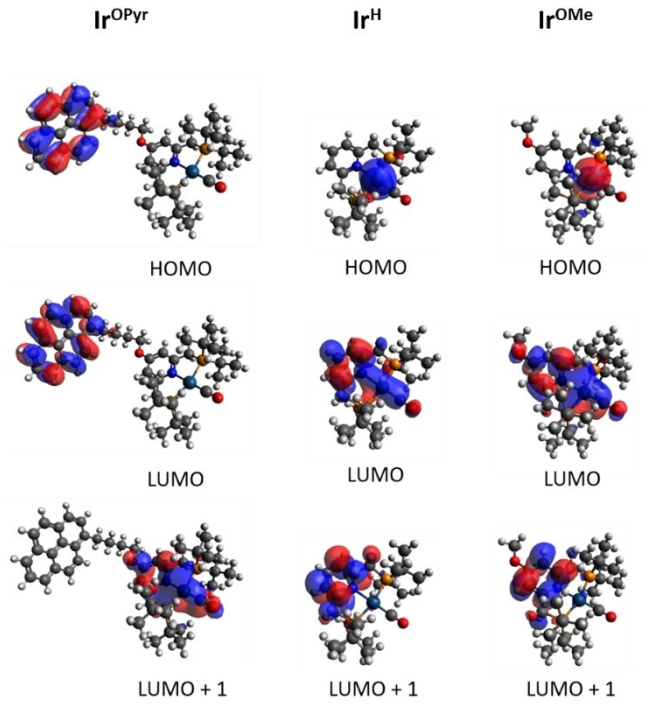

Figure 2. Calculated HOMO, LUMO and LUMO + 1 geometries for the three Ir complexes investigated.

PNP ligand framework, indicating that the one-electron reduction is both metal- and ligand-based in good agreement with the analysis reported by Brudvig et al.[15] The second reduction is predicted to be much more energetic for these two complexes, since the LUMO + 1 is 0.61–0.88 eV upward the LUMO, and accordingly it is not observed in the CVs. Conversely, in **Ir^{OPyr}** the LUMO and LUMO + 1, localized over the pyrene moiety and over the {(PNP)Ir} unit respectively, are almost degenerated ($\Delta_{LUMO\text{-}LUMO+1} = 106$ meV), which is in agreement with the observation of two successive one-electron reductions in the CV (even if the sequence of the two processes is not properly predicted at the level of DFT calculations used here).

CO_2RR electrocatalysis in DMF solution

As a preliminary step prior to heterogenize the **Ir^{OPyr}** complex, its electrocatalytic properties were investigated in homogeneous conditions and compared to those of the parent **Ir^{H}**[15] and **Ir^{OMe}** species to evaluate the effect of adding the pyrene moiety. Adapting the previously reported conditions,[15] the potential activity of **Ir^{OPyr}** to drive CO_2RR was first probed by CV using 0.5 mM solutions of the complex in DMF, under Ar or CO_2 saturated atmosphere, both in the absence and in the presence of water (4.6 M) as a source of protons. As shown in Figure 3, after saturating the mixture with CO_2, an increase of the current intensity is observed close to the cathodic system corresponding to the {(PNP)Ir} reduction. This observation is coherent with the occurrence of a catalytic process, pointing towards CO_2RR.

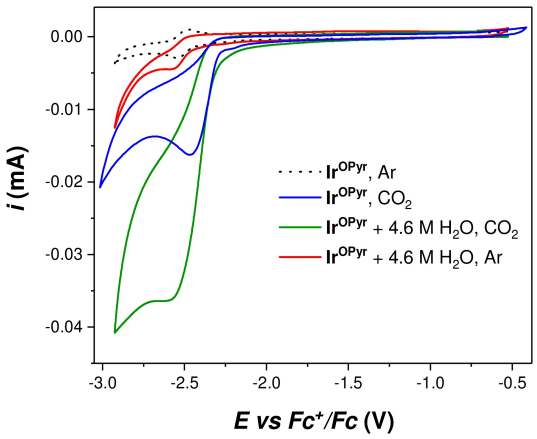

Figure 3. Cyclic voltammograms of **Ir^{OPyr}** (0.5 mM) in DMF 0.1 M nBu$_4$NPF$_6$ under argon (dotted black), under argon in the presence of H_2O (red) and under CO_2 in the absence (blue) and presence (green) of H_2O: 1.6 mm diameter GC working electrode, 100 mV·s^{-1} scan rate.

This is further supported by the drastic increase in the intensity of the catalytic peak at $E_{cat/2} = -2.40$ V upon addition of 4.6 M H_2O. Importantly, after purging the latter solution with Ar, the catalytic wave is no longer observed, thus confirming that it can be mostly attributed to CO_2RR and not to the hydrogen evolution reaction (HER) at the CV timescale.

A rinse test was performed to exclude that surface-confined species were responsible for the catalytic activity observed (see Supporting Information, Figure S3): after recording a CV in the presence of 0.5 mM **Ir^{OPyr}** in DMF 0.1 M nBu$_4$NPF$_6$ + 4.6 M H_2O under CO_2, the GC electrode was gently washed with DMF and used again as the working electrode in a fresh electrolyte solution in the absence of the complex (DMF 0.1 M nBu$_4$NPF$_6$ + 4.6 M H_2O under CO_2). The resulting CV did not display any catalytic wave, confirming that the active species for CO_2RR is homogeneous as previously observed for **Ir^{H}**.[15]

When comparing the CV recorded for **Ir^{OPyr}** vs **Ir^{OMe}** or **Ir^{H}** under CO_2 in DMF 0.1 M nBu$_4$NPF$_6$ + 4.6 M H_2O (Figure 4, Table 3

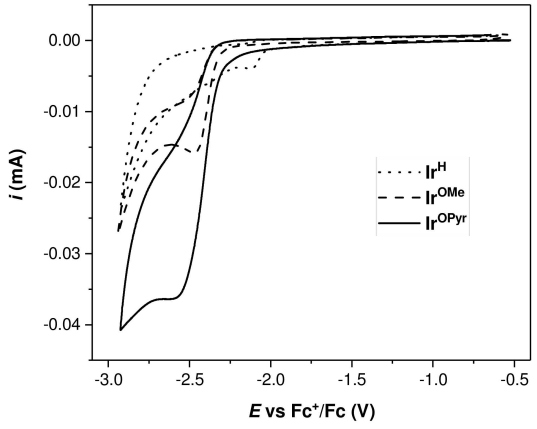

Figure 4. CVs of the three Ir complexes investigated (0.5 mM) in DMF 0.1 M nBu$_4$NPF$_6$ under CO_2 saturated atmosphere in the presence of 4.6 M H_2O (1.6 mm diameter GC working electrode, 100 mV·s^{-1} scan rate).

Table 3. Electrochemical CO_2RR parameters obtained from CV data.

Catalyst	$E_{cat/2}$ [V][a]	i_{cat}/i_p [b]	$\Delta\eta_{HCOO^-}$ [mV][c]
$\mathbf{Ir^H}$	−2.07	2.0	620
$\mathbf{Ir^{OMe}}$	−2.38	6.1	930
$\mathbf{Ir^{OPyr}}$	−2.40	13.0	950
pyrene	−2.43	3.1	980

[a] Potentials reported vs $Fc^{+/0}$. [b] i_p was measured for the first cathodic peak in the case of $\mathbf{Ir^H}$ and $\mathbf{Ir^{OMe}}$, for the pyrene reduction system in the cases of free pyrene, $\mathbf{Ir^{OPyr}}$. [c] $E^0_{DMF}CO_2/HCOO^-,H_2CO_3 = -1.45$ V vs $Fc^{+/0}$.[18]

Next, Controlled-Potential Electrolysis (CPE) experiments were carried out in DMF in the presence of 4.6 M H_2O containing 0.1 M nBu$_4$NPF$_6$ supporting electrolyte, for 0.5 mM solutions of $\mathbf{Ir^H}$, $\mathbf{Ir^{OMe}}$, $\mathbf{Ir^{OPyr}}$, and pyrene. A mercury working electrode was employed to limit both the background H_2 production and the potential formation of catalytically active metallic nanoparticles over time. For all the systems we run CPE at −2.43 V vs $Fc^{+/0}$, which corresponds roughly to the middle of

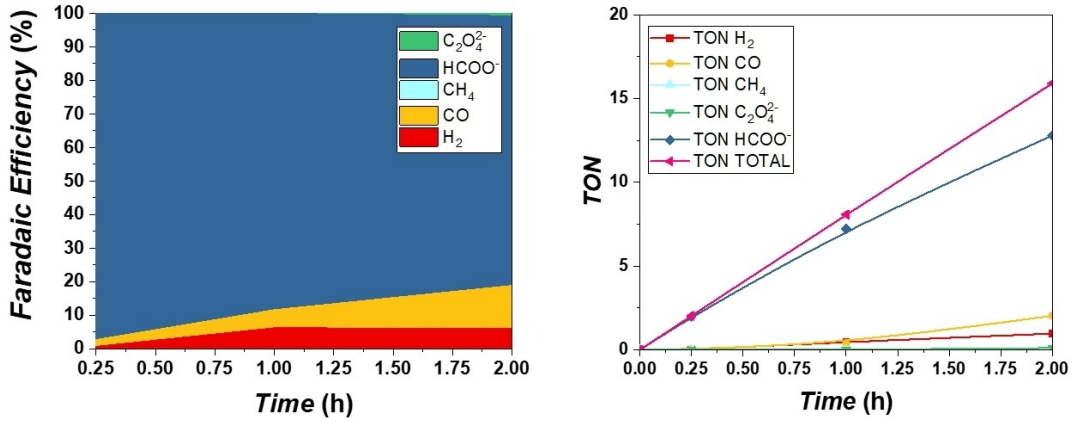

Figure 5. Faradaic efficiency (FE, left) and TON (right) for the CO_2 reduction products and hydrogen evolved during 2 h CPE experiments run at −2.43 V vs $Fc^{+/0}$, in the presence of 0.5 mM solutions of $\mathbf{Ir^{OPyr}}$ in DMF 0.1 M nBu$_4$NPF$_6$ containing 4.6 M H_2O under CO_2-saturated atmosphere (Hg working electrode).

and Figures S4 and S5), the higher apparent catalytic activity of the pyrene-derivate is striking: i_{cat}/i_p of 13.0 at $E_{cat/2} = -2.40$ V for $\mathbf{Ir^{OPyr}}$ vs 6.1 at $E_{cat/2} = -2.38$ V for $\mathbf{Ir^{OMe}}$, and 2.0 at $E_{cat/2} = -2.07$ V for $\mathbf{Ir^H}$. It should be noted that at the CV timescale the behavior of the $\mathbf{Ir^H}$ complex recorded under CO_2 in our experiments is similar to the previously reported data.[15] The catalytic overpotentials for $HCOO^-$ production, which is the main product under the present conditions (see Controlled-Potential Electrolysis data below), have been calculated to be (Table 3):[18] $\eta(\mathbf{Ir^{OPyr}})_{HCOO^-} = 950$ mV, $\eta(\mathbf{Ir^{OMe}})_{HCOO^-} = 930$ mV, and $\eta(\mathbf{Ir^H})_{HCOO^-} = 620$ mV. As expected, the values of $\eta(\mathbf{Ir^{OPyr}})_{HCOO^-}$ and $\eta(\mathbf{Ir^{OMe}})_{HCOO^-}$ are higher than $\eta(\mathbf{Ir^H})_{HCOO^-}$, due to the higher donor character of the corresponding ligands.

In an attempt to rationalize the apparent superior catalytic rates of $\mathbf{Ir^{OPyr}}$ observed at the CV timescale, the combination of the following elements can be considered:

1) The presence of the electron rich RO− substituent in *para* position of the pyridine moiety that favorably tunes the electronic properties of the complex, as suggested by the higher value of i_{cat}/i_p for $\mathbf{Ir^{OMe}}$ compared to $\mathbf{Ir^H}$ (6.1 vs 2.0, respectively, see Table 3).
2) The covalent linkage between the RO-substituted {(PNP)Ir} and the pyrene moieties in $\mathbf{Ir^{OPyr}}$, which probably act in synergy to trigger catalysis ($i_{cat}/i_p(\mathbf{Ir^{OPyr}}) = 13.0$). We suggest that the close reduction potentials of the two units allow pyrene, which in its free form also exhibits an apparent modest CO_2RR activity ($i_{cat}/i_p = 3.1$), to play the role of electron mediator in the system.

the catalytic wave observed in the CVs of the $\mathbf{Ir^{OR}}$ complexes. When running 2 h CPE, fairly stable currents were observed in most of the cases (see Figures S7–11 for the chronoamperometry profiles). The products resulting from CO_2RR and the competitive proton reduction reaction were quantified by gas (CO, CH_4, and H_2) and ionic chromatography ($HCOO^-$, $C_2O_4^{2-}$). Among all products tested, CH_4 could not be detected in any significant amounts and will not be further discussed in the following.

The evolution of the products' distribution during CPE is displayed as a function of time in Figure 5 in the case of $\mathbf{Ir^{OPyr}}$. Tables 4 and 5 summarize the 2 h long CPE results obtained in homogeneous conditions for all the systems investigated.

In our case, a different selectivity was observed for $\mathbf{Ir^H}$ complex than originally reported by Brudvig *et al.* under very

Table 4. Faradaic efficiency (FE) for all products identified during CPE experiments run at −2.43 V vs $Fc^{+/0}$ under a CO_2 saturated atmosphere, in DMF 0.1 M nBu$_4$NPF$_6$ in the presence of 4.6 M of H_2O, using a Hg working electrode.

Species	Charge [C]	FE[%] CO	FE[%] H_2	FE[%] $HCOO^-$	FE[%] $C_2O_4^{2-}$
Blank	−9.47	6	5	–	–
$\mathbf{Ir^H}$	−13.98	20	9	71	<1
$\mathbf{Ir^{OMe}}$	−11.55	16	6	79	<1
$\mathbf{Ir^{OPyr}}$	−10.75	13	6	80	<1
Pyrene	−12.36	3	4	4	–

Performed on 0.5 mM solutions (10 mL). Total CPE time: 2 h.

Table 5. Turnover numbers (TON) for all products identified during CPE experiments run at −2.43 V vs $Fc^{+/0}$ under CO_2 saturated atmosphere, in DMF 0.1 M nBu_4NPF_6 in the presence of 4.6 M H_2O, using a Hg working electrode.

Species	TON CO	TON H_2	TON $HCOO^-$	TON $C_2O_4^{2-}$
$\mathbf{Ir^H}$	5	2	18	<1
$\mathbf{Ir^{OMe}}$	3	1	14	–
$\mathbf{Ir^{OPyr}}$	2	1	15	<1
Pyrene	<1	<1	<1	–

Performed on 0.5 mM solutions (10 mL). Total CPE time: 2 h.

similar conditions:[15] we found $HCOO^-$ as the main product of CO_2 reduction with a FE of 71%, whilst the complex was reported to be selective for CO production under all potentials tested in the original work. In order to determine if this variation of selectivity could be associated to the different nature of the electrode material employed (mercury *vs* carbon), we repeated the experiment using carbon paper as working electrode (see Supporting Information, Table S1, S2, Figure S12) in otherwise identical conditions. Interestingly, in this case both CO and $HCOO^-$ were obtained with similar FE (25% and 34%, respectively), and the proportion of H_2 produced increased significantly (41% FE, Table S1). The discrepancy with the previous report can tentatively be rationalized by considering the coexistence of competitive, almost isoenergetic CO_2RR pathways, where minor modifications of the reaction conditions (electrode material, substrates/catalyst concentrations, temperature, etc.) favor one over the other(s). Nevertheless, the formation of $HCOO^-$ as the main product of CO_2RR in both cases agrees well with the known ability of iridium–pincer complexes to form metal–hydride adducts prone to CO_2 insertion[12–14,19] via an ET_H mechanism.[4] Isomerization of the metal-formate species involved in the ET_H route, to a hydroxycarbonyl intermediate of a competitive ET_M pathway,[4] can be envisaged under the Brudvig conditions, leading to CO release together with water as a side product. It is worth noting that a similar behavior was previously reported in the case of ruthenium catalysts.[20]

Looking at Table 4, we observe that for all three Ir complexes investigated, the main product of CO_2RR is invariably $HCOO^-$ (71% for $\mathbf{Ir^H}$, 79% for $\mathbf{Ir^{OMe}}$, and 80% for $\mathbf{Ir^{OPyr}}$), while CO (20% for $\mathbf{Ir^H}$, 16% for $\mathbf{Ir^{OMe}}$, and 13% for $\mathbf{Ir^{OPyr}}$) is obtained as a side product. Many other electrocatalysts have been previously reported for the selective production of $HCOO^-$ from CO_2 in homogeneous solution, based on various transition metals (Ir, Ni, Pt, Rh, Mn, Fe, Ru, Co) and supported by a variety of common ligands (porphyrins, polypyridyl ligands, aza-macrocycles, pincers, etc.).[4]

We can note that all the iridium catalysts studied here lead to relatively close product distribution. The calculated FE of $HCOO^-$, CO, and H_2 production remain in the range of 70–80%, 10–20%, and 5–10%, respectively, indicating only a minor effect of the substitution of the ligand scaffold on the selectivity of the complexes for CO_2RR in this case. Importantly, only a minor evolution of product distribution is observed over time (see Figure 5), which suggests that the catalytic systems remain fairly stable over time and that the contribution of potentially degraded species in the process is low to negligible in most of the cases.[22]

Heterogenization and electrocatalysis in water

After ensuring that the catalytic activity for CO_2RR of $\mathbf{Ir^{OPyr}}$ was preserved with respect to those of the parent catalysts $\mathbf{Ir^H}$ and $\mathbf{Ir^{OMe}}$, we next explored its activity in fully aqueous solutions. With this purpose, we immobilized $\mathbf{Ir^{OPyr}}$ on multi-walled carbon nanotubes (MWCNTs) electrodes through non-covalent π-π stacking interactions with the pyrene anchoring group. More specifically, an ink was prepared by sonication of MWCNTs in acetonitrile followed by the addition of $\mathbf{Ir^{OPyr}}$ and Nafion as binder. The ink obtained was then deposited on glassy carbon (GC) electrode, which was then washed with acetonitrile to remove any nonspecifically bound complex, then dried. The amount of iridium incorporated in the $\mathbf{Ir^{OPyr}}$@MWCNTs/GC hybrid material was determined by ICP-OES to be 1.70% (w/w) corresponding to a catalyst loading of 0.76 $\mu mol \cdot cm^{-2}$ and 47% grafting yield of the complex on MWCNTs. The chemically-modified electrodes were then evaluated for CO_2RR electrocatalysis in water (CO_2-saturated aqueous 0.5 M $KHCO_3$ solution, pH = 7.4), and compared to bare MWCNTs deposits probed under identical conditions.

The CVs of electrodes coated with $\mathbf{Ir^{OPyr}}$@MWCNTs exhibited slightly higher cathodic currents under CO_2 as compared to bare MWCNTs deposits, in the range between −0.8 to −1.2 V *vs* Ag/AgCl (Figure 6), which suggests moderate CO_2RR activity of the $\mathbf{Ir^{OPyr}}$@MWCNTs/GC hybrids in water.

Next, we run 2 h CPE experiments to confirm that the CO_2RR activity was indeed maintained, and to compare the selectivity of $\mathbf{Ir^{OPyr}}$ after heterogenization in these conditions. Based on the CV, the applied potential was fixed at −1.10 V vs Ag/AgCl, corresponding to −1.63 V vs $Fc^{+/0}$, for both $\mathbf{Ir^{OPyr}}$@MWCNTs and bare MWCNTs deposits. This corresponds to a ~860 mV anodic shift compared to the same catalytic system studied in organic

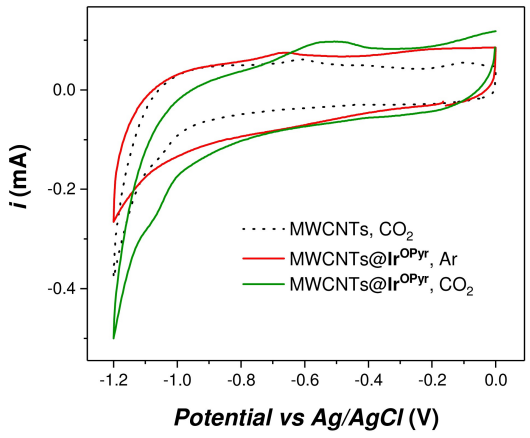

Figure 6. Cyclic voltammograms in 0.5 M $KHCO_3$ of MWCNTs/GC under CO_2 (dotted black), $\mathbf{Ir^{OPyr}}$@MWCNTs/GC under argon (red) and $\mathbf{Ir^{OPyr}}$@MWCNTs/GC under CO_2 (green).

medium ($E_{cat/2} = -2.40$ V vs $Fc^{+/0}$). Such an anodic shift of the catalytic reduction potential for CO_2RR (+450 mV) was previously reported in the case of a Ni–cyclam complex after its immobilization on carbon electrodes, via π-π interactions,[8b] and was attributed to the strong interactions between the complex and the electrode surface. In the present system, either a similar explanation and/or the stabilization of critical catalytic intermediate(s) in aqueous media can be proposed. Further investigations would, however, be required to conclude on the origin of the significant shift observed in the case of **Ir^{OPyr}**.

Table 6. Faradaic efficiency (FE) results for CPE experiments ran at −1.10 V vs Ag/AgCl (CO_2 saturated atmosphere, 0.5 M $KHCO_3$(aq), modified-1.6 mm GC working electrode).

Species	Charge [C]	FE[%] CO	FE[%] H_2	FE[%] $HCOO^-$	FE[%] $C_2O_4^{2-}$
Ir^{OPyr}@MWCNTs	−0.38	2	21	60	17
MWCNTs	−0.08	<1	99	–	–

Potentials reported vs Ag/AgCl, 3 M KCl, total time: 2 h. [a] no Nafion.

Table 7. Turnover numbers (TON) for 2 h CPE experiments (CO_2 saturated atmosphere, 0.5 M $KHCO_3$(aq), modified-1.6 mm GC working electrode).

Species	TON CO	TON H_2	TON $HCOO^-$	TON $C_2O_4^{2-}$
Ir^{OPyr}@MWCNTs	3	27	76	22

Potentials reported *vs* Ag/AgCl, 3 M KCl, total time: 2 h.

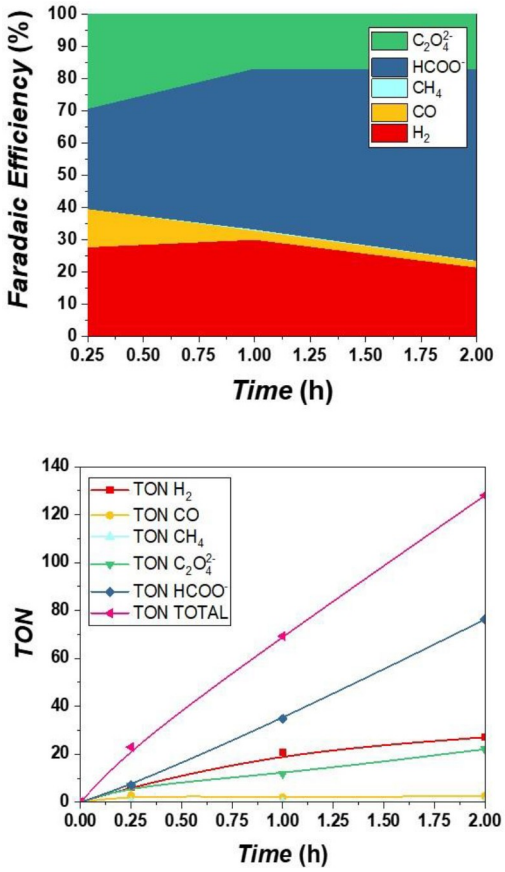

Figure 7. Faradaic efficiency (FE, top) and TON (bottom) for the reaction products observed during 2 h CPE experiments ran at −1.10 V vs Ag/AgCl using a GC working 1.6 mm electrode modified with **Ir^{OPyr}**@MWCNTs in 0.5 M $KHCO_3$(aq) under CO_2 saturated atmosphere.

The charge passed during CPE of **Ir^{OPyr}**@MWCNTs/GC hybrids is significantly higher than complex-free MWCNTs/GC (see Table 6), suggesting that the CO_2RR activity of the complex is maintained within the hybrid electrode. Furthermore, fairly stable currents were observed during the CPE (see Figure S19). The FE and TON obtained for **Ir^{OPyr}**@MWCNTs/GC and bare MWCNTs/GC are reported in Tables 6–7, the evolution of the products distribution as a function of time is displayed in Figure 7. It should be noted that TON were determined based on the total amount of Ir catalyst incorporated in the working electrode, as determined by ICP-OES, and not on its accessible electroactive fraction. This choice implies that TON reported in Table 7 are likely underestimated.

Notably, **Ir^{OPyr}** retains an activity for CO_2RR in water, leading primarily to the release of $HCOO^-$, as observed in homogeneous organic solutions, as well as for the Brookhart Ir pincer complexes.[12–14] The faradaic efficiency for $HCOO^-$ production reaches 60% after 2 hours, which makes the present system a rare example of significant production of $HCOO^-$ from CO_2 in aqueous conditions (FE >50%) catalyzed by an immobilized transition-metal complex. To the best of our knowledge, this was only previously reported for electropolymerized $[Ru(bpy)(CO)_2]_n$ films,[23] or after immobilization of the above-mentioned Brookhart Ir–pincers[14] or Mn(bipyridine) complexes[2b] onto carbon nanotubes.

The only other secondary CO_2RR products found in our heterogeneous system are $C_2O_4^{2-}$ (FE 17%) and CO (FE 2%). The presence of a significant amount of oxalate among the products of catalysis is compatible with the concurrent activation of a ET_M[4] or an outer-sphere[21] pathway.

Interestingly, when considering the evolution of the FE over time (Figure 7) we can observe a limited variation of the products distribution suggesting a relatively stable system. We can mostly note a slight decrease in the competitive processes to the benefit of $HCOO^-$ production, most likely due to slight modification of the microenvironment of the catalytic centers (local proton gradient buildup, dehydration of the Nafion film….) rather than to the evolution of the Ir complexes themselves under turnover conditions.

This hypothesis is supported by the X-ray photoelectron spectroscopy (XPS) analysis of **Ir^{OPyr}**@MWCNTs modified electrodes before and after 2 h CPE experiments ran at −1.10 V vs Ag/AgCl, which shows almost identical signatures for both the Ir and P contributions of the complexes (see Figures 8 and S33–34). The initial spectra recorded before CPE show the expected doublet from Ir^I species in the iridium 4f region at 61.9 eV ($4f_{7/2}$), together with a shoulder attributed to an Ir^{III} species at 62.6 eV ($4f_{7/2}$). Similar signatures are recorded on pristine **Ir^{OPyr}** powder, for which the ^1H and ^{31}P NMR spectra exclude the presence of Ir^{III} co-products. The unexpected Ir^{III} species are, thus, most likely generated *in situ* by exposure to X-ray radiation as recently reported for other hybrid materials featuring Ir^I centers.[24] The phosphorus region features a P $2p_{3/2}$

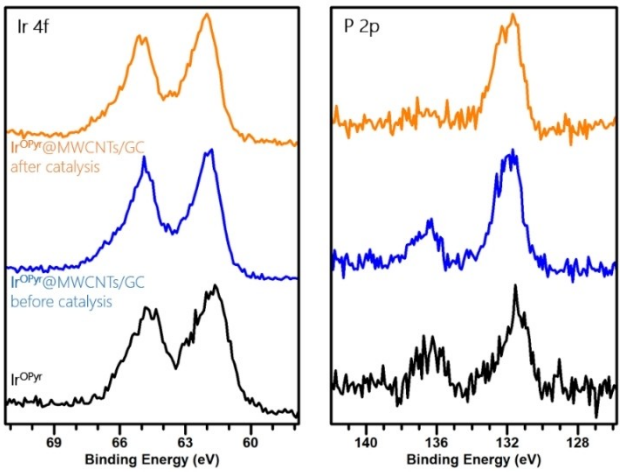

Figure 8. High resolution XPS spectra for Ir 4f (left) and P 2p (right) regions for **Ir^{OPyr}** (bottom) and **Ir^{OPyr}**@MWCNTs/GC before (middle) and after (top) CPE experiments. The signal centered around 137 eV in the P region corresponds to the PF_6^- counter-ion initially associated to the pristine **Ir^{OPyr}** complex. See Figure S34 for the peaks deconvolution.

peak at 131.7 eV (Figure S34) related to the coordinated phosphine ligands as well as another one at 136.4 eV corresponding to the PF_6^- counter-ions. By comparing the relative intensities of XPS peaks, a P/Ir ratio of 1.98 is obtained. This observation agrees perfectly with the expected stoichiometric phosphine:Ir ratio in **Ir^{OPyr}** and, thus, indicates that the integrity of the complex is preserved upon grafting. Most importantly, the XPS spectrum recorded after 2 h turnover reveals the same pattern in both the Ir 4f region ($4f_{7/2}$ at 62.0 eV) and the P 2p one (P $2p_{3/2}$ at 131.9 eV), while maintaining a P/Ir ratio of 2.02. The latter is a definitive evidence of the retention of the initial molecular structure of the catalyst under catalytic conditions.

Concluding Remarks

We have synthesized a new PNP–pincer ligand tagged with a pyrene anchoring group (**PNP^{OPyr}**), which can find general application for the heterogenization of metal–pincer complexes onto carbon-based materials and their application for small molecules activation electrocatalysis. As a study-case we have used this ligand to heterogenize a previously reported pincer–iridium complex (**Ir^{H}**), known to catalyze the electrochemical CO_2 reduction reaction.[15]

In homogeneous water/DMF mixtures the CO_2RR selectivity of the pyrene-tagged Ir catalyst (**Ir^{OPyr}**), as well as that of the pyrene-free counterparts including the original **Ir^{H}** complex, was found to differ from the previous studies: the main CO_2 reduction product being invariably $HCOO^-$ instead of CO. This observation may be related to iridium-formate and hydroxycarbonyl intermediates close in energy, which could allow switching selectivity by subtle variations of the experimental conditions.

After immobilization of **Ir^{OPyr}** on MWCNTs, the system still demonstrates a bias for CO_2RR over HER in pure water. Under these conditions, the CO_2 to $HCOO^-$ reduction activity is retained, which represents a rare case of significant formate production from CO_2 in aqueous conditions catalyzed by immobilized molecular complexes. We can also observe (i) the high stability of the catalyst under turnover conditions, as demonstrated by XPS measurements performed on the immobilized catalyst before and after CPE, and (ii) a surprisingly large anodic shift in the catalytic reduction potential for CO_2RR. The latter can be tentatively attributed to a strong interaction of the complex with the carbon surface or the stabilization of critical catalytic intermediates in fully aqueous media, even if a severe structural rearrangement of the catalyst cannot be excluded at this point.

Our current efforts are focused on the exploration of the electrochemical CO_2RR abilities of other metal–pincer complexes with pyridine-based PNP ligands, which could be successfully immobilized on electrode surfaces via π-π stacking interactions by employing the pyrene-tagged **PNP^{OPyr}** ligand.

Experimental Section

General methods. 1-(4-bromo)-pyrene,[25] diethyl 4-hydroxypyridine-2,6-dicarboxylate,[26] ^{MeO}PNP,[27] $[Ir(coe)_2(acetone)_2]PF_6$,[28] and [Ir-(^{H}PNP)CO]PF_6 (**Ir^{H}**)[15] were prepared according to literature procedures. 1,4-diazabicyclo[2.2.2]octane (DABCO) was thoroughly dried under reduced pressure before use. THF was distilled over Na/benzophenone, toluene over Na, and MeOH over CaH_2. All solvents were degassed under argon before use. All other reagents and solvents for synthesis were commercially available (analytical grade) and were used without further purification. N,N-dimethylformamide for electrochemistry was purchased from Acros Organics (99.8% Extra Dry), *n*-tetrabutylammonium hexafluorophosphate (≥99.0%) from Sigma-Aldrich, $KHCO_3$ (+99.7%) from Thermo-Fisher Scientific, MWCNTs (NC7000) from Nanocyl. N_2 (99.998%) and Ar (99.9999%) employed for catalytic experiments were purchased from Air Products or Air Liquide and used without additional purification. CO_2 (ultra-pure) was purchased from Air Liquide and used without additional purification.

All the syntheses were carried out under an atmosphere of argon by using standard Schlenk techniques (most of the organic compounds) or in a nitrogen-filled glovebox (synthesis of **5**, iridium complexes), while the purification procedures were performed under air atmosphere, with the exception of the isolation of compound **5**.

^{1}H NMR (400 MHz), ^{31}P{^{1}H} (162 MHz) and ^{11}B{^{1}H} NMR (128 MHz) spectra were recorded on a Bruker Avance III 400 MHz spectrometer in suitable solvent, and spectra were referenced to residual solvent (^{1}H) or external standard (^{31}P{^{1}H}: H_3PO_4). The infrared spectra were recorded on an Agilent Technologies Cary 630 FTIR spectrometer equipped with a standard transmission module, a diamond ATR one, and a DialPath sample interface. The low-resolution mass spectra were recorded either on an Amazon speed ion trap spectrometer or a LXQ type Thermo Scientific spectrometer, both equipped with an electrospray ionization source (ESI). The samples were analyzed in positive ionization mode by direct perfusion in the ESI-MS interface (ESI capillary voltage = 2 kV, sampling cone voltage = 40 V). The high-resolution mass spectra were recorded on a LTQ Orbitrap XL Thermo Scientific spectrometer equipped with an ESI source.

Emission spectra were recorded in deoxygenated solvents at room temperature using a Fluoromax 4 (Horiba). The iridium content was determined on an ICP-OES ACTIVA Jobin Yvon apparatus from solutions obtained by treatment of the material with sulfuric acid and aqua regia in a Teflon reactor at 400–450 °C. Milli-Q water was purified through a Millipore system.

The amounts of evolved hydrogen, carbon monoxide and methane were determined by sampling 50 µl of the headspace in Perkin Elmer Clarus 580 gas chromatograph equipped with a molecular sieves 5 Å column (30 m–0.53 mm), a methanizer and thermal conductivity (TD) and flame ionization (FI) detectors. Formate and oxalate anions were determined by ionic exchange chromatography (883 Basic IC, Metrohm).

X-ray photoelectron spectroscopy (XPS) analyses were carried out with a Versa Probe II spectrometer (ULVAC-PHI) equipped with a monochromatic Al Ka source (hν = 1486.6 eV) at CEA Grenoble. The core level peaks were recorded with constant pass energy of 23.3 eV. The XPS spectra were fitted with CasaXPS 2.3 software using Shirley background. Binding energies are referenced with respect to the adventitious carbon (C 1 s BE = 284.8 eV).

*Synthesis of diethyl 4-(4-(pyren-1-yl)butoxy)pyridine-2,6-dicarboxylate (**1**).* A mixture of 1-(4-bromo)-pyrene (2.05 g, 6.08 mmol, 1 eq), diethyl 4-hydroxypyridine-2,6-dicarboxylate (1.62 g, 6.77 mmol, 1.1 eq), dry K_2CO_3 (5.10 g, 36.90 mmol, 6.07 eq) in MeCN (60 mL) was refluxed overnight. After cooling down, $CHCl_3$ (200 mL) and Na_2CO_3 (aq sat, 100 mL) were poured into the reaction mixture. The organic phase was separated, and the aqueous layer was washed with $CHCl_3$ (2×100 mL). The organic extracts were gathered, dried with Na_2SO_4 and concentrated to dryness. The residue was purified by recrystallization in hot EtOH, dried and collected as a white powder (**1**, 1.92 g, 64% yield). IR (ATR, cm^{-1}): 2948w, 2876w, 1740s (C=O), 1711 s (C=O), 1589 m, 1560w, 1430w, 1367 m, 1339 m, 1280w, 1245 m, 1219 s, 1154 m, 1097 m, 1019 s, 948w, 842 s, 781 m, 764 m. ^{1}H NMR (400 MHz, $CDCl_3$): δ 8.27 (d, J = 9.3 Hz, 1H, *CH* pyrene), 8.17 (m, 2H, *CH* pyrene), 8.12 (m, 2H, *CH* pyrene), 8.03–7.97 (m, 3H, *CH* pyrene), 7.89 (d, J = 7.7 Hz, 1H, *CH* pyrene), 7.75 (s, 2H, *CH* pyridine), 4.46 (q, J = 7.1 Hz, 4H, C(=O)O–CH_2–CH_3), 4.18 (t, J = 5.8 Hz, 2H, CH_2), 3.45 (t, J = 7.2 Hz, 2H, CH_2), 2.12–1.98 (m, 4H, CH_2), 1.44 (t, J = 7.1 Hz, 6H, CH_3). ESI-MS (0.05 mM in MeOH, *m/z*, I %): 496.2, 100 $[MH]^+$.

*Synthesis of (4-(4-(pyren-1-yl)butoxy)pyridine-2,6-diyl)dimethanol (**2**).* Solid $LiBH_4$ (0.46 g, 21.12 mmol, 8.3 eq) was added in small portions to a suspension of **1** (1.27 g, 2.56 mmol, 1 eq) in THF/MeOH 5/2 (21 mL), pre-cooled to 0 °C in a Schlenk flask directly connected to an oil bubbler. The mixture was then left to warm to room temperature, and subsequently heated at 60 °C for 1 h. A partial solubilization was observed, as well as a strong release of H_2 bubbles from the oil bubbler. After cooling down, water (120 mL) was slowly added to the reaction mixture, resulting in the formation of a milky precipitate. The latter was filtered, washed with excess water and diethyl ether (30 mL), dried and collected as a white powder (**2**, 1.00 g, 95% yield). IR (ATR, cm^{-1}): 2570–3530w br (OH), 2947w, 2917w, 2876w, 1605 m, 1573w, 1455w, 1367w, 1350w, 1332 m, 1154 m, 1053 m, 1034 m, 842 s. ^{1}H NMR (400 MHz, d_6-DMSO): δ 8.38 (d, J = 9.3 Hz, 1H, *CH* pyrene), 8.29–8.20 (m, 4H, *CH* pyrene), 8.13 (m, 2H, *CH* pyrene), 8.06 (t, J = 15.2 Hz, 1H, *CH* pyrene), 7.99 (d, J = 7.8 Hz, 1H, *CH* pyrene), 6.86 (s, 2H, *CH* pyridine), 5.33 (br, 2H, *OH*), 4.45 (s, 4H, CH_2–OH), 4.16 (m, 2H, CH_2), 3.41 (m, 2H, CH_2), 1.93 (br, 4H, CH_2). ESI-MS (0.05 mM in MeOH, *m/z*, I%): 412.1, 100 $[MH]^+$.

*Synthesis of (4-(4-(pyren-1-yl)butoxy)pyridine-2,6-diyl)bis(methylene) bis(4-methylbenzenesulfonate) (**3**).* To a suspension of **2** (0.74 g, 1.80 mmol, 1 eq) in THF (20 mL), freshly ground KOH (0.25 g, 7.20 mmol, 4 eq), and TsCl (0.86 g, 7.20 mmol, 4 eq) were successively added. The reaction was refluxed for 20 h. After concentration under vacuum, the residue was taken up in dichloromethane (20 mL) and washed with water (2×15 mL). The organic phase was dried over Na_2SO_4 and concentrated. The crude product was purified by vacuum column chromatography.[29] (silica gel, 100% cyclohexane to 100% AcOEt gradient in 5% steps) and isolated as a beige solid (**3**, 1.00 g, 77% yield), which was directly used in the following step without further purification. ^{1}H NMR (400 MHz, $CDCl_3$): δ 8.28 (d, J = 9.3 Hz, 1H, *CH* pyrene), 8.17 (t, J = 7.2 Hz, 2H, *CH* pyrene), 8.13 (d, J = 8.6 Hz, 2H, *CH* pyrene), 8.03 (m, 2H, *CH* pyrene), 7.99 (t, J = 7.5 Hz, 1H, *CH* pyrene), 7.89 (d, J = 7.7 Hz, 1H, *CH* pyrene), 7.77 (d, J = 8.3 Hz, 4H, *CH* Ts), 7.28 (d, J = 8.1 Hz, 4H, *CH* Ts), 6.75 (s, 2H, *CH* pyridine), 4.93 (s, 4H, CH_2–OTs), 3.99 (t, J = 6.2 Hz, 2H, CH_2), 3.43 (t, J = 7.6 Hz, 2H, CH_2), 2.39 (s, 6H, CH_3), 2.09–1.91 (m, 2H, CH_2).

*Synthesis of 2,6-bis((di-tert-butylphosphanyl-borane)methyl)-4-(4-(pyren-1-yl)butoxy)pyridine (**4**).* *n*-BuLi (1.2 mL, 1.75 mmol, 5 eq, 1.46 M in hexane, freshly titrated)[30] was added to a solution of borane di(tert-butyl)phosphine complex (0.28 g, 1.75 mmol, 5 eq) in THF (10 mL), previously cooled to −78 °C. After stirring at RT for 20 min, the reaction medium was again cooled to −78 °C, and a solution of **3** (0.25 g, 0.35 mmol, 1 eq) in dichloromethane (5 mL) was added. The reaction mixture was then left to warm to RT and stirring was continued overnight. The reaction medium was then quenched with water (2 mL) and the solvents were evaporated. The crude product was purified by vacuum column chromatography (silica gel, 100% cyclohexane to 100% AcOEt gradient in 5% steps) and isolated as a beige solid (**4**, 0.20 g, 83% yield). IR (ATR, cm^{-1}): 2947w, 2917w, 2867w, 2370w br (BH), 1743w br, 1592 m, 1568 m, 1367w, 1331 m, 1153 m, 842 s. ^{1}H NMR (400 MHz, $CDCl_3$): δ 8.30 (d, J = 9.2 Hz, 1H, *CH* pyrene), 8.17–8.10 (m, 4H, *CH* pyrene), 8.04–7.96 (m, 3H, *CH* pyrene), 7.90 (d, J = 7.8 Hz, 1H, *CH* pyrene), 7.07 (br, 2H, *CH* pyridine), 4.11 (t, J = 6.1 Hz, 2H, CH_2), 3.41 (t, J = 7.3 Hz, 2H, CH_2), 3.19 (d, $J_{P\text{-}H}$ = 12 Hz, 2H, CH_2–P), 2.07–1.94 (m, 4H, CH_2), 1.28 (d, $J_{P\text{-}H}$ = 13 Hz, 18H, CH_3). ^{31}P{^{1}H} NMR (162 MHz, $CDCl_3$): δ 46.7 (s). ^{11}B{^{1}H} NMR (128 MHz, $CDCl_3$): δ −41.9 (br). ESI-MS (0.05 mM in CH_2Cl_2, *m/z*, I%): 696.4, 100 $[MH]^+$.

*Synthesis of 2,6-bis((di-tert-butylphosphaneyl)methyl)-4-(4-(pyren-1-yl)butoxy)pyridine (**PNP^{OPyr}**).* A solution of DABCO (370 mg, 3.30 mmol, 15.3 eq) and **4** (122 mg, 0.215 mmol, 1 eq) in toluene (4 mL) was heated at 80 °C for 48 h. The reaction completion was confirmed by ^{31}P{^{1}H} NMR analysis (s, 34.9 ppm). After cooling down, the solvent was removed in vacuo and the residue was extracted with pentane (3×10 mL), washed with MeOH (5 mL), filtered, dried and collected as a white powder. (**5**, 87 mg, ~60% yield). IR (ATR, cm^{-1}): 2940 m, 2888 m, 2859 m, 1585 s, 1563 s, 1487w, 1419w, 1385w, 1364 m, 1329 m, 1185w, 1149 s, 1039 s, 1014w, 977w, 840vs, 754 m, 707 s. ^{1}H NMR (400 MHz, CD_2Cl_2): δ 8.33–7.91 (9H + 9H, *CH* pyrene, main + minor species), 7.09 (s, 2H, *CH* pyridine, minor species), 6.75 (s, 2H, *CH* pyridine, main species), 4.19 (m, 2H, *CH2* minor species), 4.06 (m, 2H, *CH2* main species), 3.45–3.41 (m, 2H + 2H + 4H, *CH2* main + minor species, *CH2*–P minor species), 2.90 (d, J = 2.6 Hz, 4H, *CH2*–P main species), 3.18 (s, 2H, *CH2*–P), 2.08–1.94 (m, 4H + 4H, *CH2*, main + minor species), 1.17–1.09 (m, 36H + 36H, *CH3*, main + minor species). ^{31}P{^{1}H} NMR (162 MHz, CD_2Cl_2): δ 42.5 (s, minor species), 34.9 (s, main species). The two species in the NMR spectra are attributed to the neutral (main) and protonated (minor) forms of **5**, protonation occurring in the presence of MeOH (no multiple species were observed by ^{31}P{^{1}H} NMR upon monitoring the advancement of the reaction, i.e. prior to add MeOH). ESI-MS (0.1 mM in CH_3CN, *m/z*, I%): 668.4, 100 $[MH]^+$. High resolution ESI-MS (0.05 mM in MeCN, *m/z*): calculated for $C_{43}H_{60}NOP_2$ ($[MH]^+$), 668.41501, found: 668.41355.

Typical synthesis of the Ir complexes. Solid $[Ir(coe)_2(acetone)_2]PF_6$ (110 mg, 0.163 mmol, 1 eq) was added to a solution of **5** (109 mg, 0.163 mmol, 1 eq) in acetone (10 mL) to afford a deep red solution. After 30 min, CO was bubbled onto the reaction solution, which immediately turned yellowish. After 5 min, bubbling was stopped and the solution was concentrated to dryness. The crude product was purified by flash chromatography (SiO_2, $\mathbf{Ir^{OPyr}}$: cyclohexane: ethyl acetate 6:4, $\mathbf{Ir^{OMe}}$: from cyclohexane: ethyl acetate 1:1 to pure ethyl acetate), it was dissolved in a small volume of MeCN (2–3 mL) and precipitated as a PF_6^- salt by addition of a $KPF_{6(aq,sat)}$ solution. It was filtered, washed with an excess of water and diethyl ether, dried and collected as a yellow powder.

$\mathbf{Ir^{OPyr}}$ (68% yield). IR (ATR, cm^{-1}): 2943w br, 2866w, 1952 s (CO), 1740w, 1608 s, 1551w, 1455 s, 1366 m, 1332 s, 1230 m, 1152 m, 1051 m, 833vs. ^1H NMR (400 MHz, CD_2Cl_2): δ 8.32 (d, J = 9.2 Hz, 1H, *CH* pyrene), 8.20–8.17 (m, 2H, *CH* pyrene), 8.15–8.12 (m, 2H, *CH* pyrene), 8.07–7.99 (m, 3H, *CH* pyrene), 7.92 (d, J = 7.8 Hz, 1H, *CH* pyrene), 6.99 (s, 2H, *CH* pyridine), 4.18 (m, 2H, CH_2), 3.68 (m, 4H, *CH2*–P), 3.45 (m, 2H, CH_2), 2.02 (m, 4H, CH_2), 1.39–1.35 (m, 36H, CH_3). $^{31}P\{^1H\}$ NMR (162 MHz, CD_2Cl_2): δ 72.8 (s). ESI-MS (0.05 mM in MeOH, *m/z*, I%): 888.3, 100 $[M–PF_6]^+$. High resolution ESI-MS (0.05 mM in MeOH, *m/z*): calculated for $C_{44}H_{59}IrNO_2P_2$ ($[M–PF_6]^+$), 888.36503, found: 888.36486.

$\mathbf{Ir^{OMe}}$ (70% yield). IR (ATR, cm^{-1}): 2950w, 2879w, 1956 s (CO), 1613 m, 1472 m, 1336 m, 1235w, 1060 m, 1021w, 938w, 872w, 837vs. ^1H NMR (400 MHz, d_6-acetone): δ 7.23 (s, 2H, *CH* pyridine), 4.04–4.02 (m, 4H, CH_2), 3.88 (s, 3H, CH_3–O), 1.35–1.31 (m, 36H, CH_3). $^{31}P\{^1H\}$ NMR (162 MHz, d_6-acetone): δ 73.5 (s). ESI-MS (0.05 mM in MeCN, *m/z*, I%): 646.3, 100 $[M–PF_6]^+$. High resolution ESI-MS (0.05 mM in MeCN, *m/z*): calculated for $C_{25}H_{45}IrNO_2P_2$ ($[M–PF_6]^+$), 646.25548, found: 646.25391.

Synthesis and characterization of hybrid materials. $\mathbf{Ir^{OPyr}}$@MWCNTs: MWCNTS (5.56 mg) were sonicated in anhydrous acetonitrile (1 mL) for 30 min. Then, $\mathbf{Ir^{OPyr}}$ (1.35 mg, 1.31 μmol) and a Nafion solution (5 μL, 5 wt%) were added to the mixture, which was further stirred for 2 h resulting in a black ink.

Functionalization of electrodes. $\mathbf{Ir^{OPyr}}$@MWCNTs/GC: 25 μL of the as-prepared black ink ($\mathbf{Ir^{OPyr}}$@MWCNTs, vide supra) were deposited on a glassy carbon electrode and dried for 10 min. The electrode was soaked and turned in anhydrous acetonitrile for 5 seconds to remove non-grafted $\mathbf{Ir^{OPyr}}$, and dried. Finally, a Nafion solution (5 μL, 5 wt%) was deposited and the electrode was dried. ICP-OES (w/w %): Ir, 1.70. Grafted yield: 47%.

Electrochemistry and catalytic experiments. Electrochemical experiments were performed using a SP-300 Bio-Logic potentiostat in an air-tight three-electrode cell with a Ø 1.6 mm glassy carbon disk working electrode, a Pt wire as counter electrode and an Ag/AgCl, KCl (3 M) reference electrode separated from the bulk solution by a Vycor frit. Experiments were performed under argon or CO_2 using 0.5 mM concentrations of the complexes in 3 mL anhydrous electrolyte solution. Cyclic voltammograms (CVs) were collected at a scan rate of 100 $mV\,s^{-1}$ at room temperature. The working electrode was polished before each measurement on a MD-Nap polishing pad with a 1 μm monocrystalline diamond paste, rinsed with ethanol and dried under air. Controlled potential electrolysis (CPE) experiments were carried out with mercury or carbon paper working electrodes in a two compartment H-cell, where the counter electrode compartment was separated from the compartment containing the working and reference electrodes by a fritted glass. Electrolyte solutions were 0.1 M $[n\text{-}Bu_4N]PF_6$ in anhydrous dimethylformamide and purged with argon for 10 minutes prior to use. For experiments under CO_2 atmosphere, the solution was purged with CO_2 for 45 minutes. Ferrocene was added at the end of electrochemical experiments as an internal standard. The catalytic experiments (i.e. the CPE experiments followed by the quantification of the CO_2RR products by GC/HPLC) were repeated three times and the average values of faradaic efficiency (FE) and turnover numbers (TON) are reported in Tables 4–7, S1–S2. Standard deviations are in a range of ~5% from the mean value.

Computational methods. DFT calculations were performed using ORCA program package version 4.2.1[31] using the long range and dispersion-corrected B3LYP/G hybrid functional.[32] The def2-SVP basis set was used for all atoms.[33] Calculations were performed with the presence of a solvent reaction field of dimethylformamide produced by the conductor-like polarizable continuum model (CPCM).[34]

Acknowledgements

This work is supported by the French National Research Agency in the framework of the "Investissements d'avenir" program (ANR-15-IDEX-02), the Labex ARCANE (ANR-11-LABX-003), the CBH-EUR-GS (ANR-17-EURE-0003), and the Solar-driven chemistry program (SolarN2fixation, ANR20-SODR-0004-03). J. Fize is acknowledged for fruitful discussions on chromatographic analyses, and the Plateau Synthèse Organique (PSO-DCM) for part of the ligand preparation.

Conflict of Interests

The authors declare no conflict of interest.

Data Availability Statement

The data that support the findings of this study are available in the supplementary material of this article.

Keywords: CO_2 reduction · CO_2RR · iridium(I) complexes · pincer ligands · pyrene anchor

[1] a) A. Otto, T. Grube, S. Schiebahn, D. Stolten, *Energy Environ. Sci.* **2015**, *8*, 3283–3297; b) H. Shin, K. U. Hansen, F. Jiao, *Nat. Sustain.* **2021**, *4*, 911–919; c) K. E. Dalle, J. Warnan, J. J. Leung, B. Reuillard, I. S. Karmel, E. Reisner, *Chem. Rev.* **2019**, *119*, 2752–2875.
[2] a) K. Lei, B. Yu Xia, *Chem. Eur. J.* **2022**, *28*, e202200141; b) B. Reuillard, K. H. Ly, T. E. Rosser, M. F. Kuehnel, I. Zebger, E. Reisner, *J. Am. Chem. Soc.* **2017**, *139*, 14425–14435; c) L. Sun, V. Reddu, A. C. Fisher, X. Wang, *Energy Environ. Sci.* **2020**, *13*, 374–403; d) N. Corbin, J. Zeng, K. Williams, K. Manthiram, *Nano Res.* **2019**, *12*, 2093–2125; e) X.-M. Hu, S. U. Pedersen, K. Daasbjerg, *Curr. Opin. Electrochem.* **2019**, *15*, 148–154; f) C. Sun, R. Gobetto, C. Nervi, *New J. Chem.* **2016**, *40*, 5656–5661; g) N. Elgrishi, M. B. Chambers, X. Wang, M. Fontecave, *Chem. Soc. Rev.* **2017**, *46*, 761–796; h) S. Pugliese, N. T. Huan, A. Solé-Daura, Y. Li, J.-G. Rivera de la Cruz, J. Forte, S. Zanna, A. Krief, B.-L. Su, M. Fontecave, *Inorg. Chem.* **2022**, *61*, 15841–15852; i) J. A. Mennel, H. Pan, S. W. Palladino, C. J. Barile, *J. Phys. Chem. C* **2020**, *124*, 19716–19724; j) M. Fang, L. Xu, H. Zhang, Y. Zhu, W.-Y. Wong, *J. Am. Chem. Soc.* **2022**, *144*, 15143–15154; k) Z. Weng, J. Jiang, Y. Wu, Z. Wu, X. Guo, K. L. Materna, W. Liu, V. S. Batista, G. W. Brudvig, H. Wang, *J. Am. Chem. Soc.* **2016**, *138*, 8076–8079; l) S. Sinha, R. Zhang, J. J. Warren, *ACS Catal.* **2020**, *10*, 12284–12291; m) Y. Wu, Z. Jiang, X. Lu, Y. Liang, H. Wang, *Nature* **2019**, *575*, 639–642.
[3] E. O. Eren, S. Özkar, *J. Power Sources* **2021**, *506*, 230215.

[4] N. W. Kinzel, C. Werlé, W. Leitner, *Angew. Chem. Int. Ed.* **2021**, *60*, 11628–11686; *Angew. Chem.* **2021**, *133*, 11732–11792.
[5] a) N. Kaeffer, A. Morozan, J. Fize, E. Martinez, L. Guetaz, V. Artero, *ACS Catal.* **2016**, *6*, 3727–3737; b) M. Bourrez, F. Molton, S. Chardon-Noblat, A. Deronzier, *Angew. Chem. Int. Ed.* **2011**, *50*, 9903–9906; *Angew. Chem.* **2011**, *123*, 10077–10080.
[6] M. E. Ahmed, S. Adam, D. Saha, J. Fize, V. Artero, A. Dey, C. Duboc, *ACS Energy Lett.* **2020**, *5*, 3837–3842.
[7] J. A. Mann, J. Rodríguez-López, H. D. Abruña, W. R. Dichtel, *J. Am. Chem. Soc.* **2011**, *133*, 17614–17617.
[8] a) S. Pugliese, N. T. Huan, J. Forte, D. Grammatico, S. Zanna, B.-L. Su, Y. Li, M. Fontecave, *ChemSusChem* **2020**, *13*, 6449–6456; b) F. Greenwell, G. Neri, V. Piercy, A. J. Cowan, *Electrochim. Acta* **2021**, *392*, 139015.
[9] Y. Wu, Y. Liang, H. Wang, *Acc. Chem. Res.* **2021**, *54*, 3149–3159.
[10] S. Sinha, A. Sonea, W. Shen, S. S. Hanson, J. J. Warren, *Inorg. Chem.* **2019**, *58*, 10454–10461.
[11] C. Caix, S. Chardon-Noblat, A. Deronzier, *J. Electroanal. Chem.* **1997**, *434*, 163–170.
[12] P. Kang, C. Cheng, Z. Chen, C. K. Schauer, T. J. Meyer, M. Brookhart, *J. Am. Chem. Soc.* **2012**, *134*, 5500–5503.
[13] P. Kang, T. J. Meyer, M. Brookhart, *Chem. Sci.* **2013**, *4*, 3497–3502.
[14] P. Kang, S. Zhang, T. J. Meyer, M. Brookhart, *Angew. Chem. Int. Ed.* **2014**, *53*, 8709–8713; *Angew. Chem.* **2014**, *126*, 8853–8857.
[15] G. Hu, J. J. Jiang, H. R. Kelly, A. J. Matula, Y. Wu, N. Romano, B. Q. Mercado, H. Wang, V. S. Batista, R. H. Crabtree, G. W. Brudvig, *Chem. Commun.* **2020**, *56*, 9126–9129.
[16] S. M. Kloek, D. M. Heinekey, K. I. Goldberg, *Organometallics* **2006**, *25*, 3007–3011.
[17] a) S. F. Nelsen, L. Echegoyen, D. H. Evans, *J. Am. Chem. Soc.* **1975**, *97*, 3530–3532; b) D. H. Evans, S. F. Nelsen, in *Characterization of Solutes in Nonaqueous Solvents* (Ed.: G. Mamantov), Springer US, Boston, MA, **1978**, pp. 131–154.
[18] S. Roy, B. Sharma, J. Pécaut, P. Simon, M. Fontecave, P. D. Tran, E. Derat, V. Artero, *J. Am. Chem. Soc.* **2017**, *139*, 3685–3696.
[19] a) M. Feller, U. Gellrich, A. Anaby, Y. Diskin-Posner, D. Milstein, *J. Am. Chem. Soc.* **2016**, *138*, 6445–6454; b) R. Tanaka, M. Yamashita, K. Nozaki, *J. Am. Chem. Soc.* **2009**, *131*, 14168–14169.
[20] C. W. Machan, M. D. Sampson, C. P. Kubiak, *J. Am. Chem. Soc.* **2015**, *137*, 8564–8571.
[21] C. Costentin, M. Robert, J.-M. Savéant, *Chem. Soc. Rev.* **2013**, *42*, 2423–2436.
[22] u. o. i. c. The same analysis was realized at the foot the catalytic wave for all systems (−2.23 V vs $Fc^{+/0}$), as reported in the SI (Tables S3, S4 and Figures S13–S18). Beside the expected largely reduced TON, we note a significant reduction of FE for the production of CO and HCOO− for all three complexes together with a significant increase of the FE of both H2 and oxalate.
[23] S. Chardon-Noblat, A. Deronzier, R. Ziessel, D. Zsoldos, *J. Electroanal. Chem.* **1998**, *444*, 253–260.
[24] M. König, M. Traxler, M. A. Rudolph, J. Schmidt, H. Küçükkeçeci, R. Schomäcker, A. Thomas, *ChemCatChem* **2022**, *14*, e202200811.
[25] A. J. Lampkins, E. J. O'Neil, B. D. Smith, *J. Org. Chem.* **2008**, *73*, 6053–6058.
[26] N. Rizeq, S. N. Georgiades, *Eur. J. Org. Chem.* **2016**, *2016*, 122–131.
[27] S. Kuriyama, K. Arashiba, K. Nakajima, H. Tanaka, N. Kamaru, K. Yoshizawa, Y. Nishibayashi, *J. Am. Chem. Soc.* **2014**, *136*, 9719–9731.
[28] R. Dorta, R. Goikhman, D. Milstein, *Organometallics* **2003**, *22*, 2806–2809.
[29] D. S. Pedersen, C. Rosenbohm, *Synth.* **2001**, *2001*, 2431–2434.
[30] S. C. Watson, J. F. Eastham, *J. Organomet. Chem.* **1967**, *9*, 165–168.
[31] F. Neese, *Wiley Interdiscip. Rev.: Comput. Mol. Sci.* **2012**, *2*, 73–78.
[32] a) C. Lee, W. Yang, R. G. Parr, *Phys. Rev. B* **1988**, *37*, 785–789; b) A. D. Becke, *J. Chem. Phys.* **1993**, *98*, 5648–5652.
[33] a) P. C. Hariharan, J. A. Pople, *Theor. Chim. Acta* **1973**, *28*, 213–222; b) F. Weigend, *Phys. Chem. Chem. Phys.* **2006**, *8*, 1057–1065.
[34] M. Cossi, N. Rega, G. Scalmani, V. Barone, *J. Comput. Chem.* **2003**, *24*, 669–681.

Manuscript received: January 18, 2023
Revised manuscript received: April 4, 2023
Accepted manuscript online: April 6, 2023
Version of record online: May 5, 2023